STRUCTURAL DEMONSTRATION OF AN ACTIVE BACK-FLOW FLAP UNDER WIND TUNNEL CONDITIONS

S. Opitz,
DLR-Institute of Composite Structures and Adaptive Systems, Braunschweig, Germany
A.D. Gardner, C.B. Merz, C.C. Wolf,
DLR-Institute of Aerodynamics and Flow Technology, Göttingen, Germany

Abstract

The paper presents a detailed concept for influencing dynamic stall with a surface integrated active back-flow flap on the upper side of an airfoil. The development of the flap from a basic concept to the final wind tunnel experiment is described. Special attention is paid on the selection of flap size and position, the structural concept, the actuation mechanism and the instrumentation. Further, the manufacturing procedure developed to produce a retrofit solution for an existing wind tunnel model is illustrated. The paper closes with first functional tests of actuation mechanism and instrumentation in the wind tunnel. Finally the results from wind tunnel experiments are used to validate the predicted reduction of the pitching moment peak.

1. INTRODUCTION

Dynamic stall is a well-known effect for helicopter airfoils occurring when a pitching airfoil stalls, forming separated flow in a dynamic stall vortex. A lift peak and a negative spike in pitching moment form and then a rapid drop in lift appears as the stall vortex moves downstream. The torsional impulse from the pitching moment peak is often a load-limiting case for the pitch link rods, and high drag is experienced compared to attached flow. Dynamic stall can be controlled by using passive devices, including vortex generators and changes in the leading edge contour [6, 7], but these have disadvantages at high Mach number and are limited in their control of deep stall. In contrast, active devices include actively retracting vortex generators [5], which avoid shocks at high Mach number, or air jets [11, 12], which add energy to the flow, and thus improve the flow control under deep stall conditions.

The leading-edge stall associated with many helicopter airfoils including the OA209 [1] airfoil used for the numerical predictions, is characterized by strong backward flow along the suction side of the airfoil [9]. To control dynamic stall of this type, the single dynamic stall vortex should be broken into several smaller vortices and the passage of the vortices should be delayed [2].

2. STALL CONTROL WITH A BACK-FLOW FLAP

As part of the DLR project STELAR an alternative method of influencing dynamic stall using an active back-flow flap is presently being investigated [4]. In the past back-flow flaps have been tested on gliders as a passive method of reducing stall [8], as freely-hinged spoiler-like flaps on the suction side of the airfoil near the trailing edge. When trailing edge stall occurs, the back-flow lifts the flap and the region of stall can be significantly delayed. Even though the effectiveness of back-flow flaps has been demonstrated in flight experiments with sailplanes, it still has to be investigated whether they are also suited to improve the dynamic stall behavior of helicopter rotor blades [3].

2.1. Principle of operation

Initial numerical investigations with an actively actuated flap showed promising results. The computation was performed in 2D using the unstructured DLR-TAU solver and the Spalart-Allmaras turbulence model using the settings of Richter et al. [10]. The flap was dynamically actuated to only be deployed during the stalled flow, by using the overset grid (chimera) method with automatic hole cutting. The back-flow flap breaks the main stall vortex into smaller structures, and this results in a reduction in the pitching moment peak of 34 % compared to the reference case without actuation, while maintaining the lift during the attached flow (see Figure 1).

2.2. Findings from first wind tunnel experiment

To gather first experiences, simple wind tunnel experiments were performed with an oscillating 2D airfoil

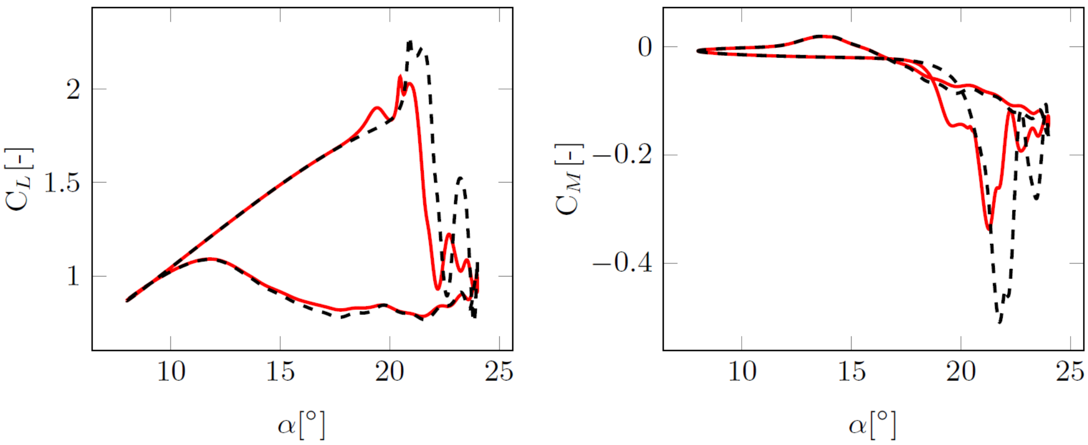

Figure 1: Comparison of lift (left) and pitching moment coefficient (right) for the OA209 airfoil at M=0.14, Re=920000, $\omega^* = 2\,\pi\,f\,c/v_\infty$=0.1, α=16±8°. The black lines are without flap actuation, and the red lines are with flap actuation (image from [4]).

without instrumentation. The model was equipped with a passive back-flow flap and the flow was monitored with tufts and a high-speed video camera (setup see Figure 2). Analyzing the results with passive flaps , it was noted that an existing airfoil could generally be retrofitted with a flow control flap. However, to have reproducible conditions during the

Figure 2: Passive back-flow flap model in the 1MG at 50 m/s. Flow is from left to right (image from [13]).

wind tunnel experiment the back-flow flap approach requires an actuator to hold the flap closed when not needed (e.g. reference cases), and to accelerate the opening of the flap with a pulse of force to guarantee the immediate flap actuation. Further, an angle restriction is needed to limit the flap opening angle, so that the highly dynamic opening of the flap does not cause the flap to flip over lying upside down upstream of the hinge line.

2.3. Basic concept

Summing up the results of the initial numerical investigations and the first wind tunnel experiment a list of requirements for the structure and the actuation mechanism was established. Based upon this list, a concept was developed and presented in detail in [13] and [14]. To prevent any steps or gaps the concept comprises a solid state hinge that connects the flap to a Glassfiber Reinforced Polymer (GFRP) shell that forms the outer model surface. Fiber reinforced elastomers that are highly bendable but do not elongate significantly under tensile loading are intended to limit the flap opening angle.
To provide the opening impulse for the flap the actuation concept uses flap integrated magnets that can be attracted or pushed away by a second set of magnets that moves underneath the GFRP shell. With this approach the flap can be held closed or swiftly opened. Even though this concept could be shown to be generally feasible there were still a lot of open questions to be answered before the final wind tunnel testing of the back-flow flap. Major points were:

- detailed aerodynamic design (size and position of the flap)
- concept for a retrofit solution of an existing wind tunnel model that is compatible with structure, actuation and instrumentation
- detailed design of actuation mechanism
- instrumentation of the wind tunnel model

These issues will be addressed within this paper, presenting a detailed concept for the retrofit of a wind tunnel model. The paper ends with initial wind tunnel results from the testing of the active back-flow flap.

3. DESIGN OF WIND TUNNEL MODEL

3.1. Aerodynamic design

Computations using the method of Kaufman et al. [4] were performed to estimate the correct size and position of the flap. Therefore the flap size was varied in 3 steps from 5 % chord to 15 % chord. The position of the flap was altered in steps of 10 % chord between 10 % and 70 % of chord. The results of this study are depicted in Figure 3. These computations represent

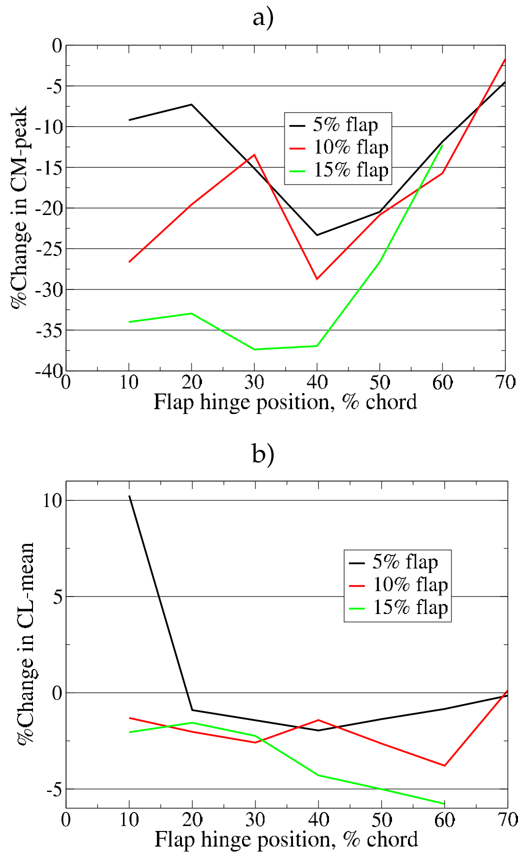

Figure 3: Numerical investigation of the flap size and position, compared to the reference case without a flap, a): Change in pitching moment coefficient peak (Dynamic stall load), b): Change in mean lift coefficient (Hysteresis).

only a rough approximation of the real physics, since they could not model the body-on-body parts of the opening, and always had a gap between the flap and the airfoil. Further, the flap motion which was prescribed in the computations would certainly differ in reality.
Nevertheless some trends can be deduced. In most cases the reduction of the pitching moment peak becomes more effective with increasing flap length. At the same time a larger flap tends to cause a larger reduction of the mean lift coefficient. In contrast to the flaps used to improve the static stall behavior of gliders, positions near the trailing edge do not seem to be effective to reduce the pitching moment peak caused by dynamic stall. For all three investigated flap lengths the best position of the flap appears to be in the range between 30 % and 50 % of chord and tends to be closer to the leading edge for larger flaps. For the two larger flap configurations the mean lift tends to decrease when the flap is shifted towards the trailing edge.
Setting the flap to a length of 15 % chord with hinge position of 30 % chord had the greatest reduction in pitching moment, while not excessively reducing lift. The demonstrator for the basic concept of the solid state hinge and the magnetic actuation concept (see [13]) had an effective flap length of approx. 35 mm which corresponds to approx. 9.5 % chord of the later wind tunnel model. Laboratory tests have shown that in this configuration the actuation mechanism is able to deploy the flap to 30° in approx. 12.5 ms. This opening speed was sufficient to match the prescribed motion that was used in the numerical investigation when the airfoil oscillates with a frequency of 6 Hz.
As the inertia of the flap rises with increasing flap size and consequently reduces the deployment speed, it was decided to realize a flap that extends over 12.5 % of the chord instead of the 15 % that gave the best results in the numerical prediction. Following the best simulated configuration the hinge line of the solid state hinge was placed at 30 % chord. Further on, the decision was made to limit the flap opening angle to a maximum of 30°, to avoid over-opening during the back-flow of the fully separated flow. On the basis of the computations a reduction of the pitching moment peak by 30 % and a loss for $C_{L_{mean}}$ of 2.5 % is expected for this setting.

3.2. Structural design

During the first wind tunnel experiment with passive flaps it was posited that it is possible to equip an existing wind tunnel model with a kind of back-flow flap glove. Such a retrofit solution has multiple advantages. If an adequate concept is found the structure and the instrumentation of an existing model can be used to save costs and to reduce the development time for each tested configuration. Additionally the potential to retrofit existing rotor blades with a back-flow flap can be demonstrated to a certain extent. The first challenge related to a retrofit solution is to find a good compromise between available installation space and size of the model. Increasing the chord length leads to a larger blockage of the wind tunnel and also to a larger flap that might be difficult to deploy in a short time due to its inertia. For this reason the developed glove should be as short and as thin

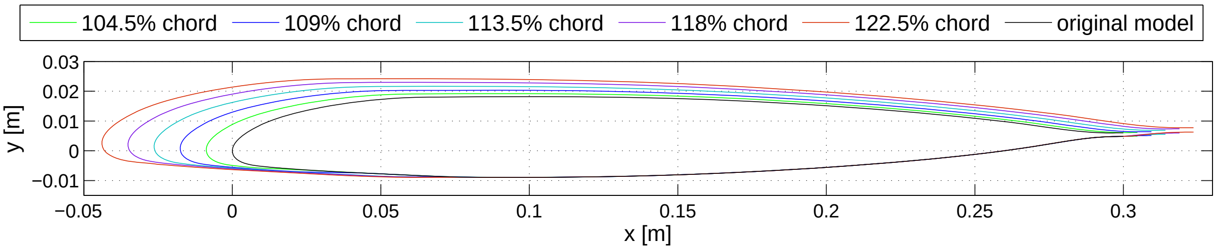

Figure 4: Positioning of the original airfoil of the wind tunnel model within the glove of the back-flow flap for different chord lengths of the modified model.

as possible. To maximize the mounting space available at the upper surface where the flap is installed, it was decided to partially use the lower side of the underlying model. The existing wind tunnel model that is intended to be equipped with the back-flow flap has a chord length of 300 mm. Already knowing the chordwise position and the size of the flap within the retrofit-glove from the aerodynamic design, a small optimization routine was used to place the original airfoil in the enlarged contour of the model with the back-flow flap. This placement was done in a way that a maximum of mounting space is available at the position of the actuation mechanism. The optimization was repeated for increasing chord length of the glove until the distance between new and old airfoil guaranteed a thickness of 5 mm at the position of the flap (see Figure 4). This requirement for a minimum thickness is driven by the size of the neodymium magnets that will be used to actuate the flap. The magnets installed in the flap and the magnets sliding underneath the GFRP-shell have a thickness of 2 mm each. Consequently a minimum of 4 mm thickness is already needed without any structure that incorporates the magnets or friction layers that enable the sliding motion and protect the underlying wind tunnel model. Finally the described optimization procedure resulted in a scale of 1.225 for the glove which is equivalent to a chord length of 367.5 mm (red line in Figure 4).

The basic concept presented in [13] and [14] already demonstrated the general compatibility of an elastomeric angle restriction with the manufacturing process and the actuation mechanism. To guarantee a reliable operation of the flap, the angle restraints for the whole model have to be sized to resist the impulsive opening forces that occur when the back-flow during dynamic stall fully opens the flap. For this purpose customized peel off tests have been performed for different interface designs between angle restraint and GFRP (see Figure 5). The elastomer of the angle restriction is reinforced with a very thin glass fiber fabric. For the connection to the GFRP structure two different configurations were investigated. Configuration 1 connects the restraint via its outer elastomer layer. For configuration 2 the glass fibers of the angle restraint were directly placed on the GFRP. Hence

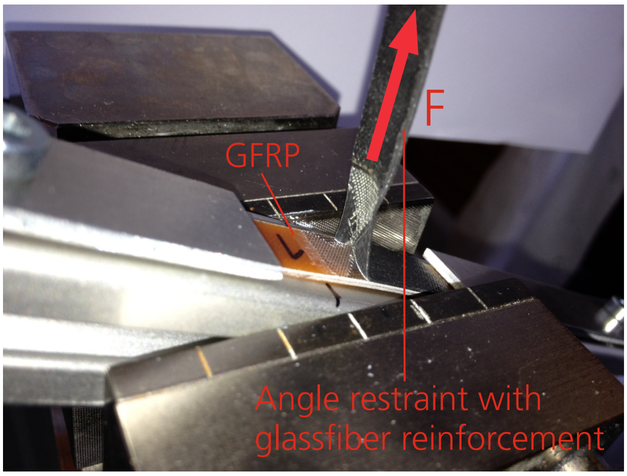

Figure 5: Customized peel off test for the design of the angle restraint

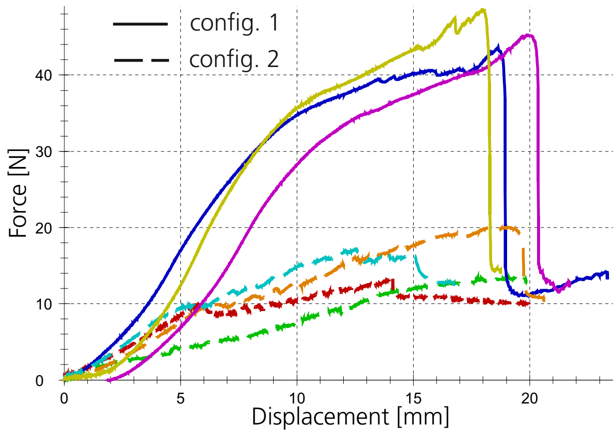

Figure 6: Peel off strength for different configurations of the interface between GFRP and angle restraint (Colors refer to different specimen).

the duromer matrix can infiltrate the glass fiber fabric. The initial intention of this measure was to benefit from the more rigid connection between restraint and GFRP that is formed when the load carrying fibers of the restraint are directly connected to the glove structure. Figure 6 depicts the force carried by the restraints over the displacement of the testing machine for both interface designs.

It is obvious that both configurations have different failure behaviors. Against the expectation all specimen from configuration 2 had a remarkably lower failure load compared to configuration 1. Due to the peel off loading, the rigid connection of the angle restraint leads to a stress concentration at the front of the bond line that causes an early failure in this region. After the first failure the stress concentration moves to the new front of the bond line and consequently causes an successive failure at a low load level. The more flexible interface that connects the glass fiber fabric through an elastomer layer distributes the load over a larger interface area and therefore prevents excessive peel stresses. Consequently higher failure loads are achieved until the initial failure of the interface. Hence configuration 1 was chosen for the final wind tunnel model.
The aerodynamic loads were roughly estimated from the numerical investigations. Finally 8 angle restraints were distributed over the span of the wind tunnel model.

3.3. Actuation

Figure 7 shows the general operation principle for the actuation mechanism of an active back-flow flap presented in [13] and [14]. The mechanism consists of

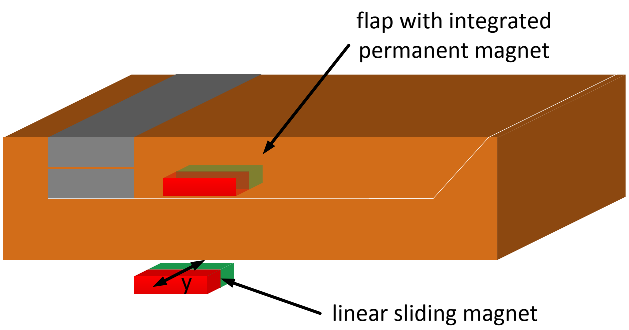

Figure 7: Actuation principle (image from [13]).

two magnets. In previous publications it was demonstrated how a magnet could be integrated into the GFRP-flap. The second, moving magnet and the adjacent actuation mechanism that generates the linear motion were not in the focus of interest so far. In [14] it is shown that the magnetic actuation system can lead to a snap opening of the flap when the bending stiffness of the solid state hinge is small. As the actuation concept allows to keep the flap closed and to deploy it, the bending stiffness of the hinge is preferred to be as small as possible, while still allowing a robust operation of the flap. This enables large opening angles since the restoring moment that has to be overcome by the magnetic forces stays small. The small bending stiffness and the nonlinear magnet forces used to deploy the flap allow the final wind tunnel model to have the same impulsive opening behavior described in [14]. This circumstance already prevents a linear control of the flap angle. Since the flap operation is digital, there is no need to have a linear control of the position of the moving magnets. This makes simple electromechanical solenoids located on both sides of the model an adequate option.
Numerical simulations of the magnetic field between the neodymium magnets in the flap and underneath the GFRP-shell have been used to estimate the repellent and attracting forces for the flap deployment and at the same time the forces that are needed to move a single magnet underneath its counterpart in the flap. Figure 8 shows these forces for a single pair of neodymium magnets. The back-flow flap of the

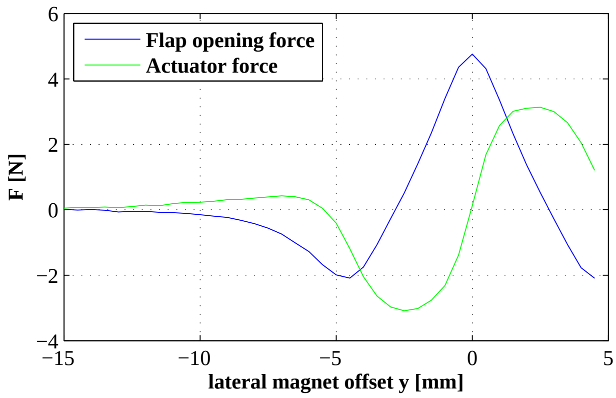

Figure 8: Actuation forces for a single pair of magnets.

wind tunnel model is deployed by 24 pairs of magnets distributed over the span of the model. According to the numerical prediction a force of approx. 75 N is needed to move all magnets in the worst case of a blocked flap that does not deploy.
To comply with the minimum of available mounting space the sliding magnets were integrated into a lightweight fiber composite push rod with a thickness of only 2.2 mm. To ensure a simultaneous motion of all magnet pairs the spacing between the magnets was adjusted to the actual spanwise location of the magnets in the flap after the manufacturing process. as the push rod exits the model in the region of the root attachment (see Figure 9), two electromechanical solenoids were used on both sides of the model. Each electromechanical solenoid is able to generate a pulling force of approximately 40 N when operated in a 25 % duty cycle. Switching to a 10 % duty cycle an increase in the voltage and current to reach forces of up to 55 N per electromechanical solenoid is possible. This leaves enough margin to compensate inertia forces or friction.
The electromechanical solenoids are controlled by a micro-controller that analyzes a sinusoidal signal that represents the pitching angle of the model to allow

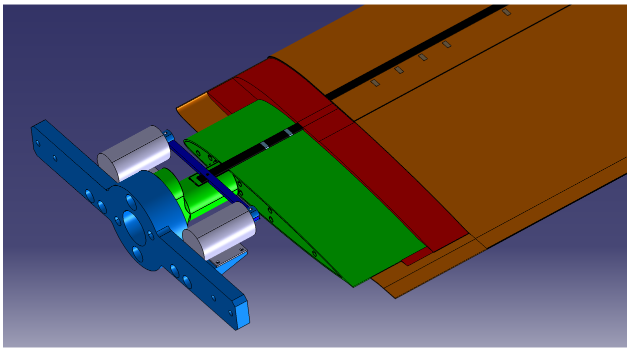

Figure 9: Retrofit-concept (green: original model, orange: GFRP-shell, red: resin, blue: model attachment, gray: electromechanical solenoids, , black: push rod).

the deployment of the flap synchronized to the model motion. The phase angle for the opening of the flap can be set by a potentiometer to tune the timing of the opening to the dynamic stall condition of each measurement point.

3.4. Instrumentation

The main purpose of the investigated back-flow flap is the reduction of the peak in pitching moment when the airfoil dynamically enters stall conditions. Therefore it is necessary to determine the forces and moments acting on the model. One possibility to determine the lift and the pitching moment during dynamic stall is the installation of pressure sensors that are distributed over the chord length of the airfoil on the upper and lower surface of the model. Integrating those pressures over the airfoil surface delivers lift, drag and pitching moment at each time step. The movable flap exhibits a challenge for this method as the orientation of the flap surface has to be regarded during the integration. Further on the pressures at the upper and lower surface of the flap have to be known.

To tackle these challenges the model was equipped with a variety of sensors. A combination of Hall effect sensors and magnets integrated into the flap are used to measure the opening angle of the flap. When the flap opens the integrated magnet moves and the sensor signal changes. A calibration curve is acquired to relate the measured voltage of the hall sensor to an opening angle of the flap.

To enable a measurement of the pressures on the upper and lower surface of the flap, five pressure tubes were integrated into the flap and connected to pressure transducers that are integrated in the rigid part of the glove.

In addition to this instrumentation the pressure sensors from the underlying model are fed through the glove. Small O-rings were used to seal between the glove and the model around each pressure measuring hole. The instrumentation is completed by a set of sensors that allow the measurement of pressures near the leading edge of the glove.

4. MANUFACTURING CONCEPT

The glove is designed to have an upper and a lower shell, that are split along the chord line of the glove profile. The manufacturing of the demonstrator can be divided into several steps and is shown for the upper part of the glove. The main process steps are depicted in Figure 10. First, the outer shell of the wind

a)

b)

c)

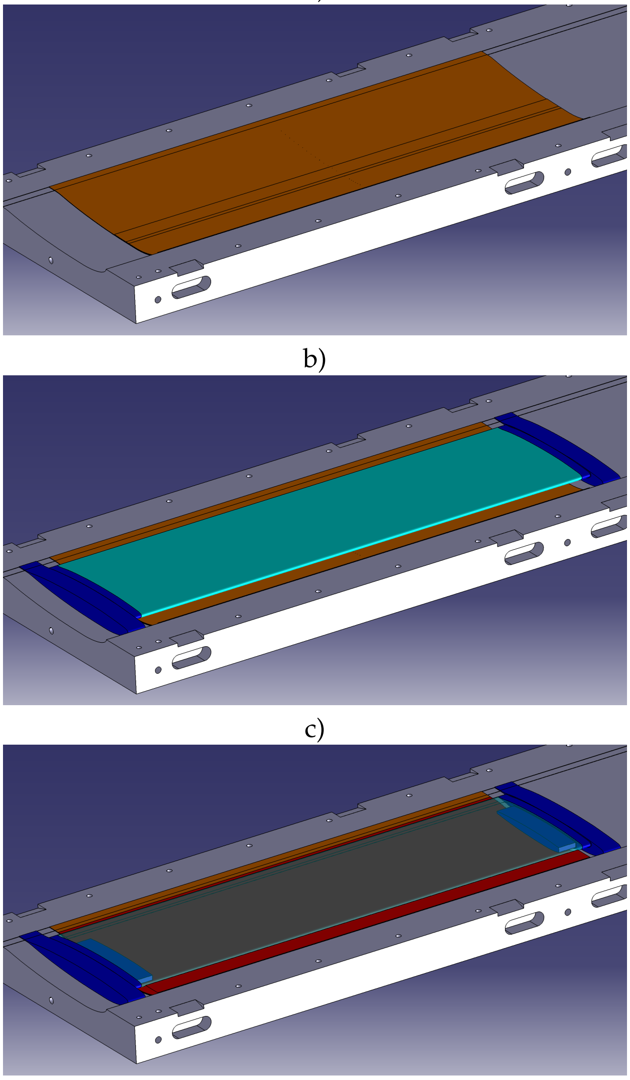

Figure 10: Major manufacturing steps.

tunnel model is manufactured (Figure 10 a)). This part is mainly made of GFRP and has different integrated functionalities. To allow a surface smooth integration of the flap an elastomeric solid state hinge is used to connect the back-flow flap with the GFRP

shell that forms the outer surface of the model. Further, the fiber reinforced elastomers for the limitation of the opening angle are also integrated. Using materials with compatible curing and vulcanization cycles as well as separating foils it was possible to manufacture all GFRP-parts and the hinge in one shot.
The fiber composite shell of the glove also comprises parts of the actuation mechanism and the instrumentation. To allow the integration of permanent magnets (actuation and flap angle measurement) a curing cycle has to be chosen that does not exceed the Curie temperature of the magnetic material.
To prevent the liquid resin from entering the pressure tubes integrated into the flap, both ends were sealed. The end at the trailing edge of the flap was permanently closed with epoxy resin. The other end of the tube is located close to the hinge point of the solid state hinge and is aligned in parallel to the hinge line in order to minimize the motion of the point where the pressure tube is later connected to the transducer via a flexible hose. During manufacturing this end is sealed using a small block of silicon. After the curing cycle the silicon can be removed. The resulting cavity can be used to contain the flexible hose that connects the pressure transducer. Finally a small hole with a diameter of 0.3 mm was drilled through the flap surface into the tube to allow the pressure measurement at this point.
After curing the composite part of the glove, the cavity between the outer shell and the underlying wind tunnel model has to be filled. For this purpose a dummy with the same geometry as the later wind tunnel model (green in Figure 9) was manufactured with a cold setting GFRP laminate. This dummy is depicted in light blue in Figure 10 b). Two positioning guides (dark blue, one on each side) were used to define the relative position between the outer surface of the glove and the dummy of the wind tunnel model. After sealing between the dummy and the GFRP-shell at both spanwise ends, the cavity was filled with a very slow cold setting casting resin (red in Figure 10 c)). This principle is repeated for the lower part of the glove. Afterwards the parting plane of the upper and lower part of the model were milled and the holes for the feed through of the pressure holes to the outer surface of the glove were drilled. The poured resin block can be used to integrate the additional pressure transducers and the Hall effect sensors as well as all kinds of wiring. Finally, the notch that guides the push rod of the actuation mechanism is also milled into the resin.
One of the major intentions for coming up with the retrofit of an existing wind tunnel model was to preserve the functionality of the original model for later investigations. Consequently a solution had to be found to temporarily mount the glove on top of the model. For this purpose different adhesive tapes were experimentally characterized with respect to their ductile behavior. Finally a transparent double-sided self-adhesive tape consisting of a PET backing and a tackyfied acrylic adhesive (tesa® 4965) were selected to mount the glove to the model. The transitions between original wind tunnel model and back-flow flap glove on the lower side of the model were sealed with silicone.

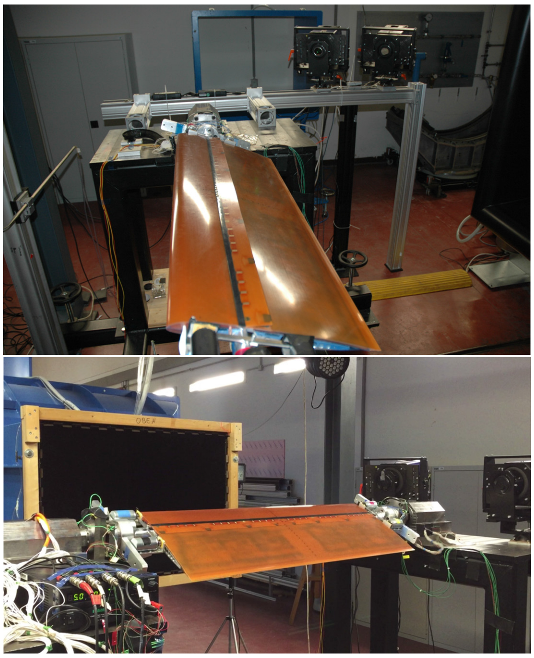

Figure 11: Model in the open test section of the wind tunnel.

5. WIND TUNNEL TESTING

The wind tunnel model with the installed back-flow flap glove is depicted in Figure 11. The model was mounted horizontally in the 1 m wide and 0.75 m high open test section of the 1MG low speed wind tunnel in Göttingen. The airfoil is supported on both sides by bearings, and driven from one side using an electromotor. In the upper picture the actuation mechanism is holding the flap open. As described in section 3.4. the forces on the airfoil were measured using the integration of pressures from the airfoil midline. Additionally a piezoelectric force balance was used as a check of the forces. The pressure integration on the airfoil includes sensors above and below the flap. The flap angle is measured by the Hall-effect sensors and is factored into the force computation. The pressure under the flap is taken to be a constant from the single pressure sensor present there, as an approximately constant pressure was indicated by the CFD computations of [4]. The pressure sensors are differential Kulites, type XCQ-093, which are referenced to the static pressure outside the free jet. To

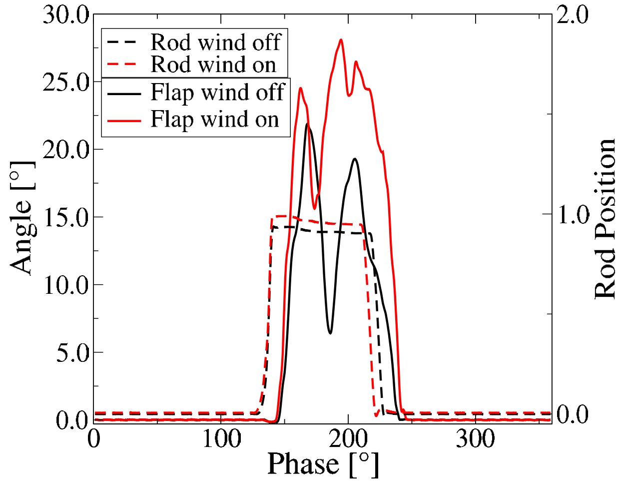

Figure 12: Influence of wind on the flap motion (α=22±8°, f=2.5 Hz, black lines: 0 m/s, red lines: 50 m/s).

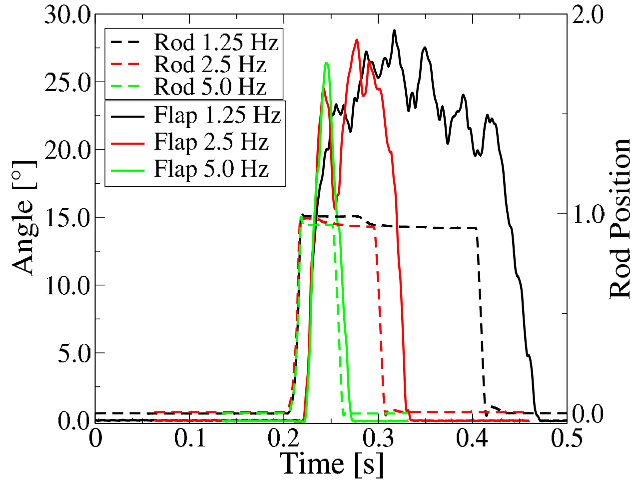

Figure 13: Influence of frequency on the flap motion (α=22±8°, wind speed 50 m/s).

compute C_P, the pressure sensors are referenced to the dynamic pressure as measured by a Prandtl-probe mounted at the nozzle exit. The Prandtl probe is also used to compute the flow speed. The position of the push rod is quantified in the same way as the flap angle using another combination of Hall-effect sensor and magnet. Therefore the permanent magnet was attached to one end of the push rod while the Hall sensor was glued to the model root attachment. The angle of attack of the airfoil is measured using two laser rangefinders, which measure to the flat plate at the bottom of the force balance. The average of the calibrated angles of attack is used.

The flap and its actuation mechanism have already been tested in the laboratory without any aerodynamic forces. Adding wind can have a strong effect on the opening behavior of the flap since the magnetic actuation mechanism exhibits no mechanical connection between push rod and flap. Further on, the whole concept relies on the utilization of the forces generated by the back-flow to fully deploy the flap. Figure 12 shows the opening of the flap with and without wind. Looking on the flap motion without wind it can be seen that the dynamic opening causes a strong oscillation of the flap angle. This is due to the characteristic of the magnetic forces. When the flap opens the repellent force between the two magnets decreases with the square of their mean distance. In the equilibrium state the moment generated by the magnetic forces equals the elastic moment that is needed to deform the solid state hinge. When the flap is dynamically opened the kinetic energy stored in the flap motion leads to an overshoot in flap angle and the flap starts oscillating around this equilibrium. Besides the motion of the flap the diagram also qualitatively shows the motion of the push rod. As expected there is no influence from the wind to the sliding motion of the magnets when the flap opens. Even though the push rod motion indicates a comparable excitation of the flap, operating the flap in the flow of the wind tunnel significantly alters the flap motion (red lines in Figure 12). It can be seen that the flap opening speed is slightly increased by the aerodynamic forces. The oscillation of the flap angle is still visible but less pronounced. After the first cycle of the flap angle oscillation the back-flow developed during dynamic stall fully opens the flap. As the angle restriction has some flexibility (also see Figure 5) the maximum opening angle is rather a soft stop than a hard limit. Comparing the phase shift between the movement of the push rod in "close" position and the reaction of the flap, reveals that the authority of the actuation mechanism to close the flap is limited. This holds especially for large opening angles where the magnetic forces are small. Aerodynamic forces can further delay the closing motion. Principally the flap closes when the flow reattaches and the magnets keep the flap closed.

To investigate the effectiveness of the flap for a large set of operating conditions, the frequency of the model pitching motion was one parameter to be varied. As the flap opening frequency has to match the model motion it has to be investigated how the frequency influences the flap motion. Figure 13 depicts the time histories of the flap angle for different actuation frequencies. In order to compare the opening behavior the curves are shifted so that the push rod motions (into the "open" position) are aligned for all three frequencies. Due to the digital snap-opening behavior of the flap (described in section 3.3.), the slope of the flap angle during opening is independent of the actuation frequency. For slow pitching motions (e.g. 1.25Hz, black line in Figure 13) the stall vortex has

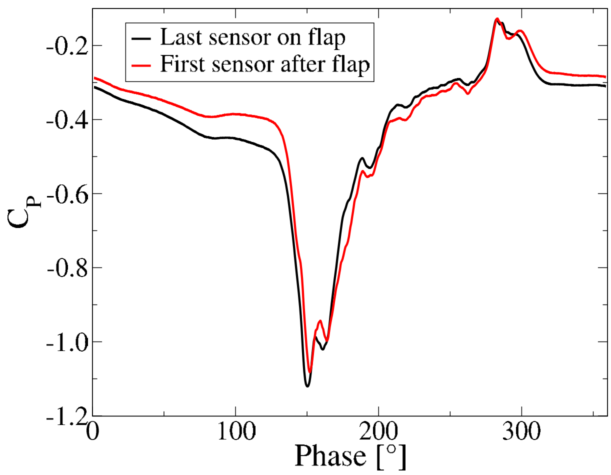

Figure 14: Validation of pressure sensor integration (α=22±8°, f=2.5 Hz, wind speed 50 m/s).

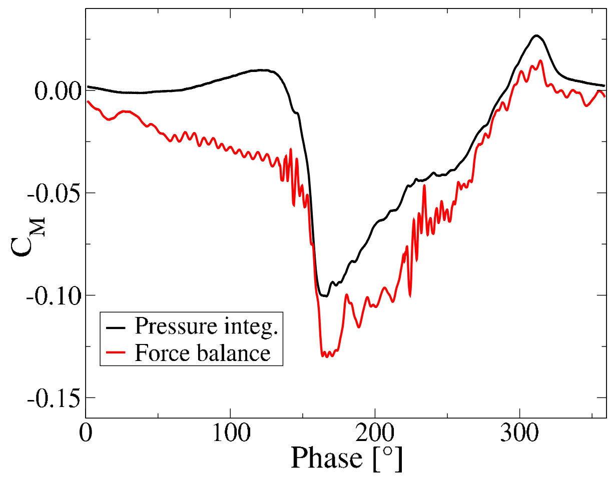

Figure 15: Moment coefficient measured with balance and integration of pressure sensor signals (α=22±8°, f=2.5 Hz, wind speed 50 m/s).

long time to form and the back-flow opens the flap for a long time. During this period the flap angle is oscillating between 20 ° and 28 °. With rising frequency the flap opening period becomes shorter and at 5 Hz it seems that the flap directly closes after the first oscillation cycle. The unsteady flap motion is therefore much less pronounced.
Two tests were performed to check the correctness of the pressure measurement on the flap surface. The first test was executed in the laboratory and addressed the deformation of the flexible hose that was used to connect the pressure tube in the flap to the transducer integrated into the glove. Therefore the measurement hole on the flap surface was closed with tape. It could be confirmed that the small deformation of the flexible hose does not generate a significant pressure signal. The second test was performed in the wind tunnel and clarified that the additional air cavity caused by the rather long pressure tube does not have a major effect on the dynamics of the sensor signal. For this purpose Figure 14 shows the comparison of the signals of a sensor near the trailing edge of the flap (longest pressure tube) and the transducer directly behind the flap. For this experiment the flap was kept closed. Hence there is no deformation of the flexible hose. A flow condition with dynamic stall was chosen for this comparison to have a clear peak in the pressure signals that allows evaluating the slope of the signal and potential phase shifts. From the figure it can be seen that both sensors show very comparable results and no significant delay or damping of the pressure signals is to be expected. The difference in the pressure signals is assumed to be only caused by the chordwise offset of the sensor position.
The motivation for emphasizing the importance of the pressure instrumentation becomes evident when the lift and moment computed from the pressures are compared to the force balance signal. The Figures 15

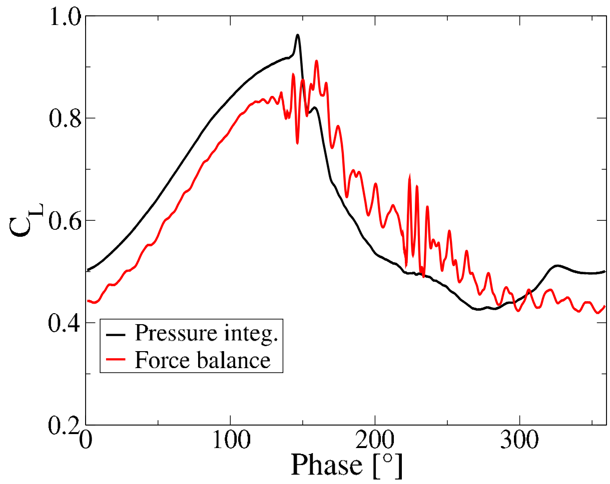

Figure 16: Lift coefficient measured with balance and integration of pressure sensor signals (α=22±8°, f=2.5 Hz, wind speed 50 m/s).

and 16 show a comparison of moment and lift coefficient determined via force balance and pressure integration. In both cases the signals from the force balance are polluted by strong interferences. Each time the flap is opened or closed the armatures of the electromechanical solenoids swiftly move into a hard stop. Therefore they are generating a strong shock force. The piezoelectric force transducers in the balance are very sensitive to this high frequency excitation. The generated oscillation of the opening and closing of the flap can be clearly recognized at a phase of 130° and 220°.
Another challenge in the post-processing of the force balance signal is the position of the model root attachment relative to the airfoil of the glove. While the original model is connected to the force balance close to the neutral point of the profile there is a sig-

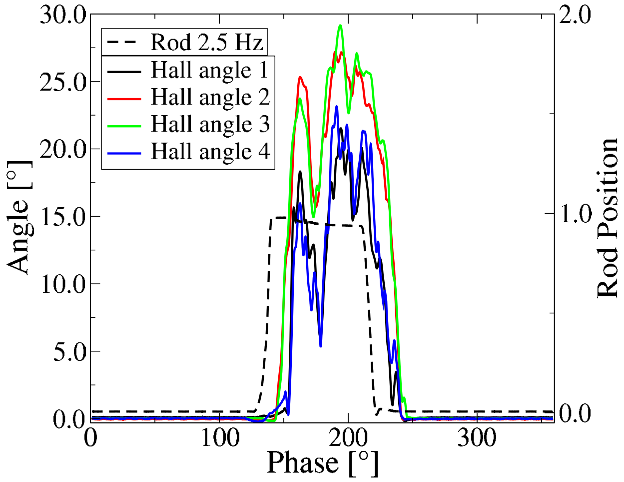

Figure 17: Flap opening angle for different span-wise locations (α=22±8°, f=2.5 Hz, wind speed 50 m/s).

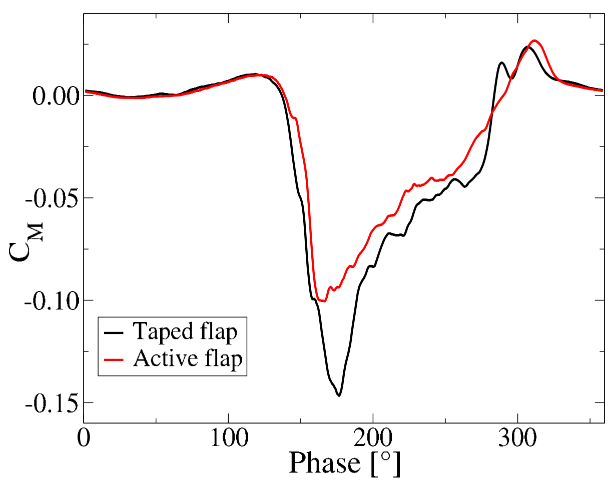

Figure 18: Example result for the influence of the back-flow flap on the pitching moment coefficient (α=22±8°, f=2.5 Hz, wind speed 50 m/s).

nificant chordwise offset between the attachment and the neutral point of the modified airfoil (also see position of original model within the glove in Figure 4). This offset requires a correction of the pitching moment as the lift is generating additional moments.
Since the model is tested in an open test section the force balance measurements are also influenced by edge effects at both spanwise ends of the model. These are the reason for the offset in lift visible in Figure 16.
As a consequence of those difficulties in the post processing of the force balance data the pressure sensor signal will be used to assess the aerodynamic effect of the back-flow flap.
The edge effects at the sides of the model also influence the flap opening. This becomes obvious when the flap angles from the 4 different spanwise positions are compared (see Figure 17). The vortexes rolling up at both sides of the model cause a delay in the flap opening. This can be directly seen in the phase shift of the flap angle from the sensors 1 and 4. The edge effect also prevents the full deployment of the flap at the side of the model. The Hall-effect sensors 2 and 3 are located closer to the airfoil midline. In this region the flap angle becomes significantly higher and the flap begins to open earlier compared to the model ends. The difference in flap angle is an indicator for the flexibility of a GFRP-flap with a thickness of 1 mm, a chord length of approx. 41 mm and a spanwise extension of 1 m. At the same time the similarity of the signals from Hall-effect sensors 1 and 4 as well as from sensors 2 and 3 give a good impression of the symmetry of the flow conditions on both ends of the model.
This paper is not intended to give a detailed insight in the behavior of the flap for a variety of flow conditions. Nevertheless one example result will be

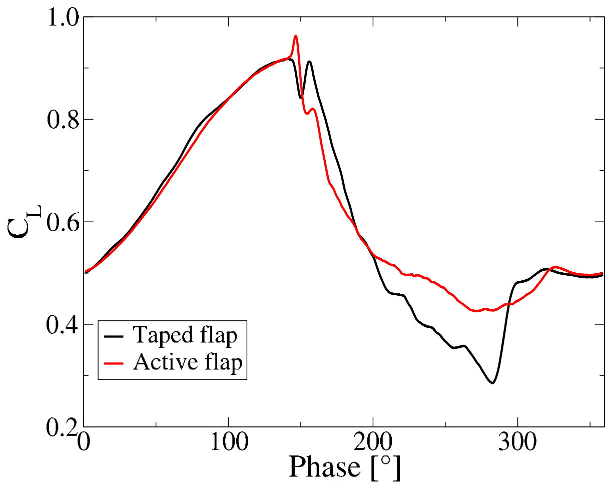

Figure 19: Example result for the influence of the back-flow flap on the lift coefficient (α=22±8°, f=2.5 Hz, wind speed 50 m/s).

presented to prove the effectiveness of the concept. Therefore the model with the flap was tested at a wind speed of 50 m/s. The airfoil was oscillating with an amplitude of 8° around a mean angle of 22° with a frequency of 2.5 Hz causing a pronounced dynamic stall. The related peak in pitching moment can be clearly recognized in Figure 18. In this deep stall condition the magnets were no longer able to keep the flap closed in each cycle. For this reason the flap was closed with tape for the reference measurement without flap actuation. During the experiment the timing for the opening of the flap was set manually to match the onset of the pitching moment peak. An online estimation of the pitching moment from a weighted sum of the pressure sensor signals enabled this procedure. For this flow condition the active back-flow flap was able to reduce the pitching moment peak by about 32 %. At the same time lift and pitching moment remained almost unchanged until the onset of the dynamic stall.

6. CONCLUSIONS

The paper presents the way from the basic principle of an active back-flow flap to the successful testing in a wind tunnel. The size and position of the flap were determined using numerical simulations. For the structural design of the wind tunnel model a solution that requires a very small mounting space for structure, actuation system and instrumentation has been presented. Based on experimental investigations the interface design for the angle restraint that limits the flap opening angle has been selected. The concepts presented for the actuation and instrumentation were successfully integrated in the manufacturing process. Finally, first wind tunnel results were able to show that the predicted reduction in the pitching moment peak of approx. 30 % can be reached, validating also the results of the numerical simulation. The expected reduction of the mean lift by approx. 2.5 % could not be confirmed by the experimental data. The wind tunnel results even show a small increase in mean lift which is beneficial for the back-flow flap concept but clearly shows the deficits of either the numerical prediction or the wind tunnel setup.

References

[1] Gallot, J., Vingut, G., De Paul, M. V., Thibert, J. "Blade profile for rotary wing of an aircraft", United States Patent 4325675,(20.4.1982).

[2] Gardner, A.D., Richter, K., Rosemann, H., "Numerical investigation of air jets for dynamic stall control on the OA209 airfoil", CEAS Aeronautical Journal, Volume 1, Issue 1, Page 69-82, 2011. DOI 10.1007/s13272-011-0002-z

[3] Höfinger, Marc, "Rotorblatt mit integrierter passiver Oberflächenklappe" Deutsches Patent DE 10 2010 041 111 A1, 22.03.2012.

[4] Kaufmann,K., Gardner, A.D., Richter, K., "Numerical Investigations of a Back-Flow Flap for Dynamic Stall Control", New Results in Numerical and Experimental Fluid Mechanics IX, Notes on Numerical Fluid Mechanics and Multidisciplinary Design, Volume 124, 2014, pp 255-262. DOI: 10.1007/978-3-319-03158-3_26.

[5] LePape, A., Costes, M., Joubert, G., David, F., Deluc, J.-M., "Experimental Study of Dynamic Stall Control Using Deployable Leading-Edge Vortex Generators", AIAA Journal, Vol. 50, No. 10 (2012), pp. 2135-2145.

[6] Mai, H., Dietz, G., Geissler, W., Richter, K., Bosbach, J., Richard, H., de Groot, K., "Dynamic stall control by leading edge vortex generators", J. Am. Helicopter Soc. 53(1), pp26-36 (2008)

[7] Martin, P., Wilson, J., Berry, J., Wong, T., Moulton, M., McVeigh, M., "Passive Control of Compressible Dynamic Stall" AIAA Paper 2008-7506, 2008.

[8] Meyer, R.K.J., "Experimentelle Untersuchungen von Rückströmklappen auf Tragflügeln zur Beeinflussung von Strömungsablösungen. Dissertation Technische Universität Berlin, Mensch-und-Buch-Verlag, 2000.

[9] Mulleners, K., Raffel, M., "The onset of dynamic stall revisited", Experiments in Fluids, Vol. 52, (3), pp 779-793, 2012. DOI 10.1007/s00348-011-1118-y

[10] Richter, K., Le Pape, A., Knopp, T., Costes, M., Gleize, V., Gardner, A.D., "Improved Two-Dimensional Dynamic Stall Prediction with Structured and Hybrid Numerical Methods" Journal of the American Helicopter Society, Volume 56, Issue 4, 2011. doi:10.4050/JAHS.56.042007

[11] Weaver, D., McAlister, K.W., Tso, J., "Control of VR7 Dynamic stall by strong steady blowing", Journal of Aircraft, Vol. 41, No. 6, 2004.

[12] Gardner, A.D., Richter, K., Mai, H., Neuhaus, D., "Experimental Investigation of Air Jets for the Control of Compressible Dynamic Stall", Journal of the American Helicopter Society, Volume 58, Number 4, 2013. DOI: 10.4050/JAHS.58.042001.

[13] Opitz, S., Gardner, A.D., Kaufmann, K., "Aerodynamic and structural investigation of an active back-flow flap for dynamic stall control", CEAS Aeronautical Journal, Vol. 5, No. 3, 2014. pp. 279-291. DOI 10.1007/s13272-014-0106-3

[14] Opitz, S., Gardner, A.D., Kaufmann, K., "An active back-flow flap for a helicopter rotor blade", Advances in Aircraft and Spacecraft Science, Vol. 1, No. 1, 2014, pp. 69-91. DOI: 10.12989/aas.2014.1.1.069.